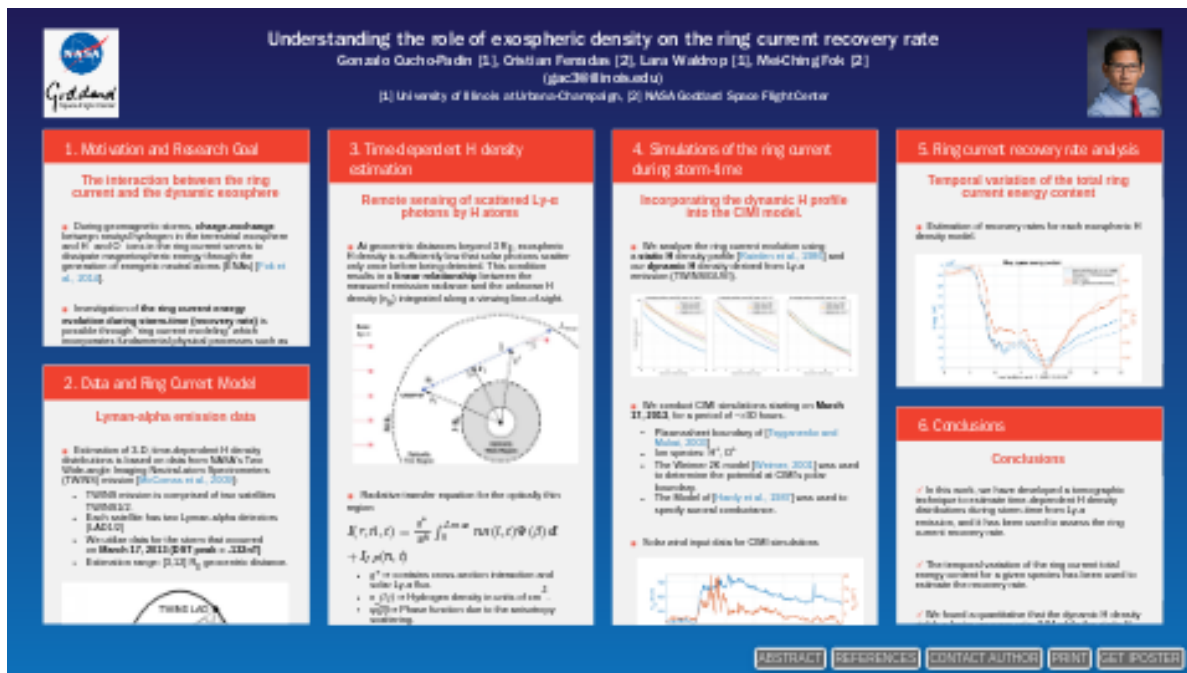


Understanding the role of exospheric density on the ring current recovery rate



Gonzalo Cucho-Padin [1], Cristian Ferradas [2], Lara Waldrop [1], Mei-Ching Fok [2]
 (gac3@illinois.edu)

[1] University of Illinois at Urbana-Champaign, [2] NASA Goddard Space Flight Center



PRESENTED AT:

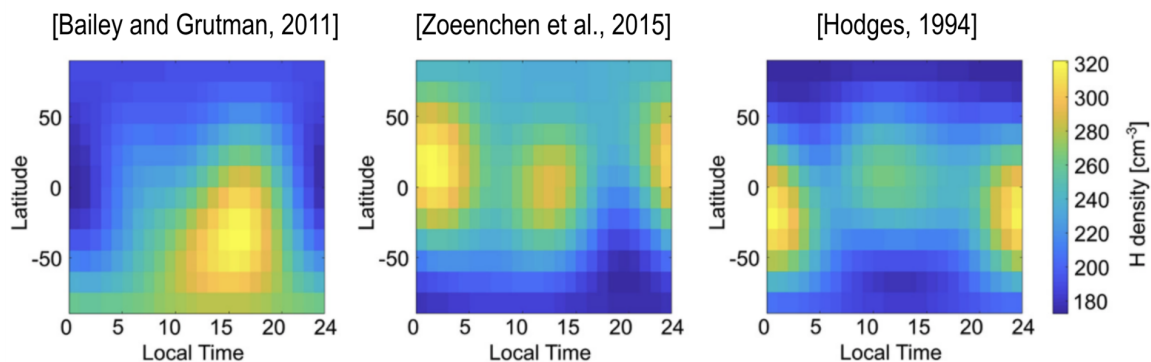


1. MOTIVATION AND RESEARCH GOAL

The interaction between the ring current and the dynamic exosphere

- During geomagnetic storms, **charge-exchange** between neutral hydrogen in the terrestrial exosphere and H^+ and O^+ ions in the ring current serves to dissipate magnetospheric energy through the generation of energetic neutral atoms (ENAs) [Fok et al., 2014 (<https://agupubs.onlinelibrary.wiley.com/doi/10.1002/2014JA020239>)].
- Investigation of the **ring current energy evolution during storm-time (recovery rate)** is possible through “ring current modeling” which incorporates fundamental physical processes such as charge-exchange, ion-ion collisions, and wave-particle interactions. However, its accuracy **depends critically on the specification of the exospheric density distributions** [Krall et al., 2018 (<https://agupubs.onlinelibrary.wiley.com/doi/full/10.1002/2017SW001780>), Illie et al., 2012 (<https://doi.org/10.1016/j.jastp.2012.03.010>)].
- The terrestrial exosphere is the uppermost layer of the atmosphere which extends from 500 km (exobase) up to $\sim 30 R_E$ (Earth radii). The atomic hydrogen (H) is the main constituent.
- Remote sensing of solar Lyman-alpha photon scattered by exospheric H atoms** (“Ly- α ” @ 121.6nm) is the only means available to estimate exospheric density distributions over such a vast region.
- Existing theoretical and data-based H density models have been generated **specifically for quiet-time conditions** whereby the assumption of a static exosphere is likely valid.

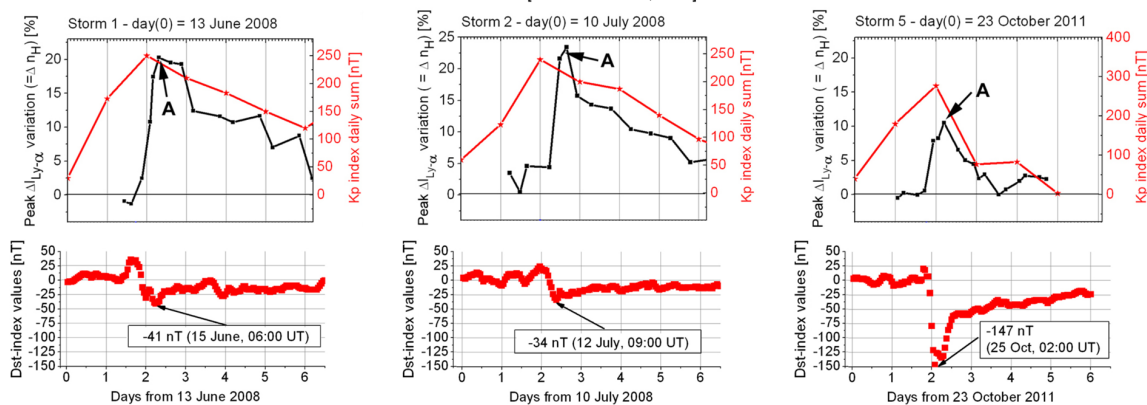
Hydrogen density distribution for a given radial shell $R = 3.2 R_E$



- Recent observations of Ly- α emission scattered by exospheric H atoms unveiled the **rapid fluctuations in their density distributions during geomagnetic storms** [Zoenchen et al., 2017 (<https://doi.org/10.5194/angeo-35-171-2017>), Kuwabara et al., 2017 (<https://agupubs.onlinelibrary.wiley.com/doi/full/10.1002/2016JA023247>)]. Such a dynamic behavior is yet to be included in those H density models.

Scattered Lyman-alpha (@121.6nm) variation during storm time

Source: [Zoenen et al., 2017]



Overarching question

What is the role of the storm-time terrestrial exosphere on the ring current recovery rate?

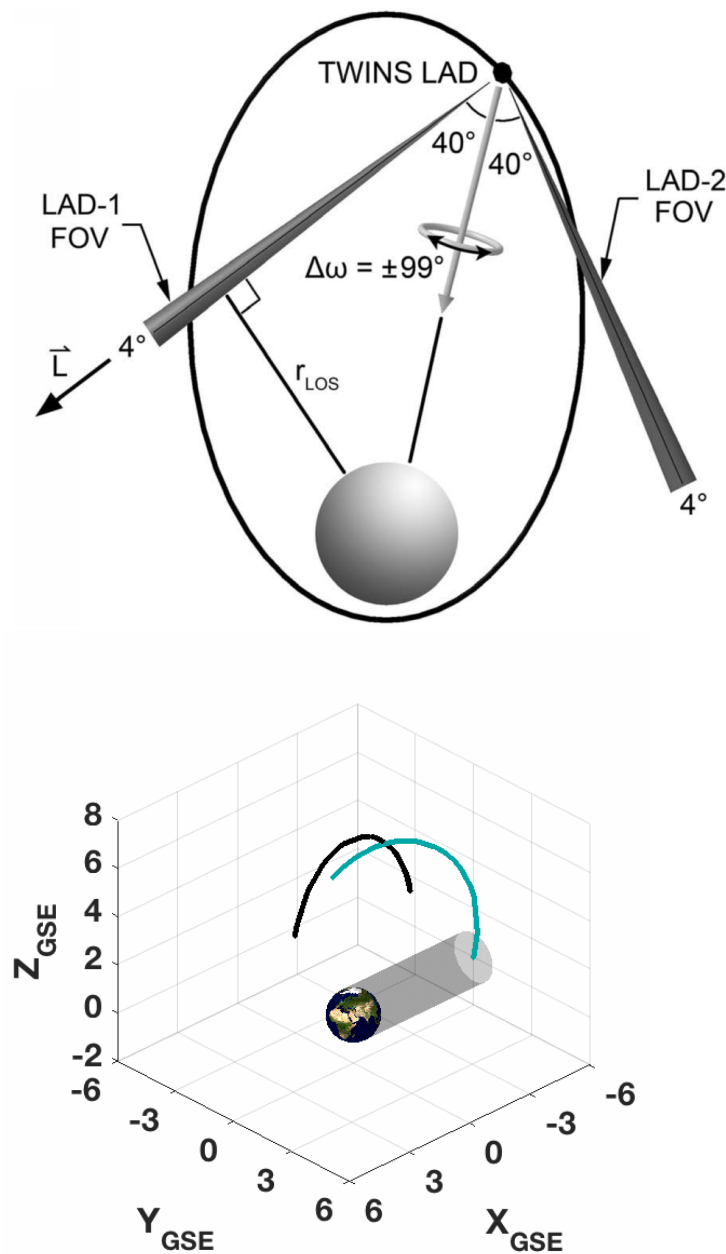
- To address this question, we estimate the 3-D, time-dependent hydrogen density distributions based on its Ly- α emission and a tomographic approach during storm-time. We then include the retrieved H density profile into a ring current model and assess the recovery rate.

2. DATA AND RING CURRENT MODEL

Lyman-alpha emission data

● Estimation of 3-D, time-dependent H density distributions is based on data from NASA's Two Wide-angle Imaging Neutral-atom Spectrometers (TWINS) mission [McComas et al., 2009 (<https://doi.org/10.1007/s11214-008-9467-4>)]:

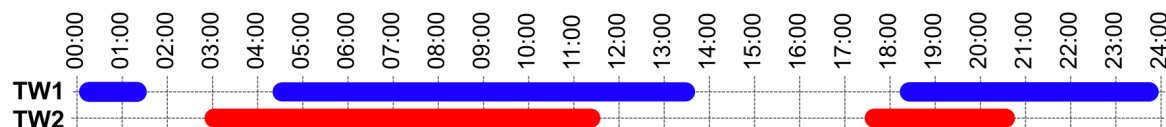
- TWINS mission is comprised of two satellites TWINS1/2.
- Each satellite has two Lyman-alpha detectors (LAD1/2)
- We utilize data for the storm that occurred on **March 17, 2013 (DST peak = -132nT)**
- Estimation range: [3,12] R_E geocentric distance.



Left panel from [Bailey and Grutman, 2011 (<https://doi.org/10.1029/2011JA016531>)]

- TWINS data availability is not continuous during the day.

TWINS data availability during March 17, 2013



- Additionally, we use data from the Global UltraViolet Imager (GUVI) on-board the Thermosphere Ionosphere Mesosphere Energetics and Dynamics (TIMED) mission to estimate an averaged and spherically symmetric H density distribution during solar-maximum conditions in the region [92, 500] km [Qin et al, 2017 (<https://doi.org/10.1002/2017JA024489>)]

- We connect both datasets (GUVI and TWINS) using a two-exponential function based on a similar procedure demonstrated by [Østgaard et al., 2003 (<https://doi.org/10.1029/2002JA009749>)] using GEO/IMAGE data.

Ring Current Model

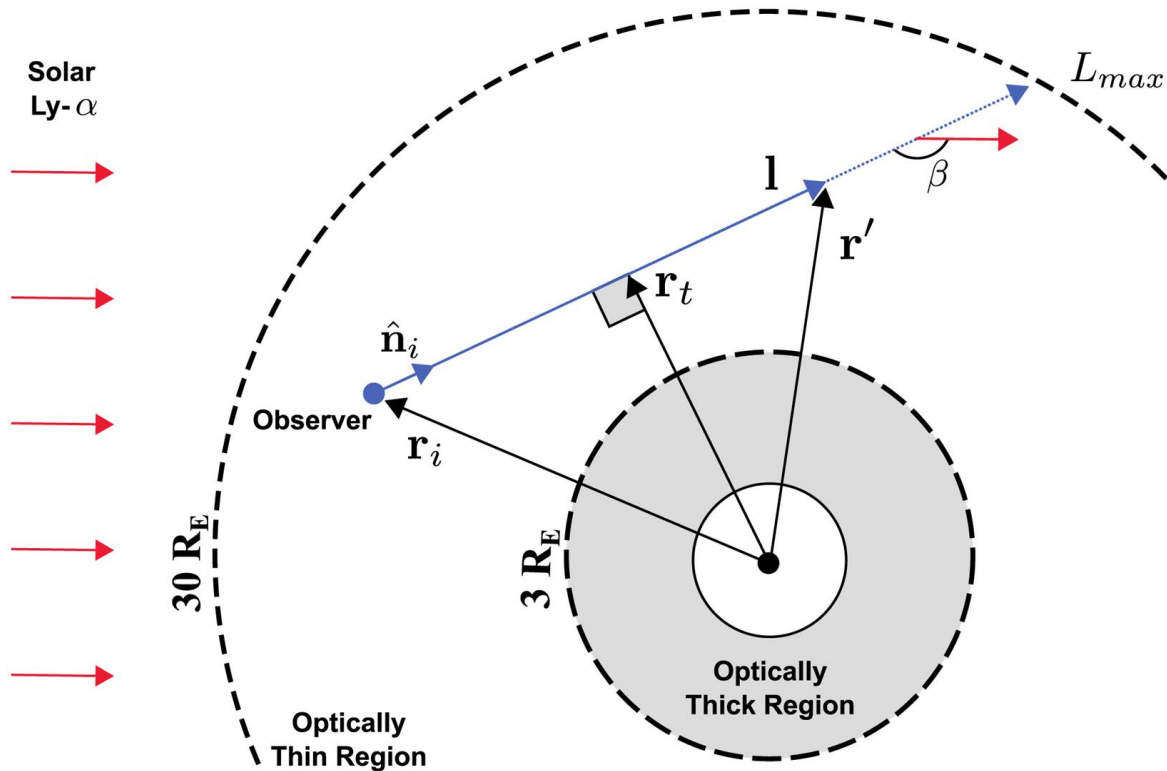
- We use the **Comprehensive Inner-Magnetosphere Ionosphere** (CIMI) model to simulate the ring current dynamics [Fok et al., 2014 (<http://agupubs.onlinelibrary.wiley.com/doi/10.1002/2014JA020239>)]

- CIMI model yield energetic ion (0.1 keV - 500 keV) and electron (1 keV - 5 MeV) distributions, Region 2 field-aligned currents, sub-auroral ionospheric potentials, and plasmaspheric densities. For this, CIMI solves:
 1. The bounce-averaged Boltzmann equation for distribution functions of ring current and radiation belt particles;
 2. The ionospheric current conservation equation for the ionospheric potential; and
 3. The equation for the total plasmasphere ion content per unit magnetic flux.

3. TIME-DEPENDENT H DENSITY ESTIMATION

Remote sensing of scattered Ly- α photons by H atoms

At geocentric distances beyond $3 R_E$, exospheric H density is sufficiently low that solar photons scatter only once before being detected. This condition results in a **linear relationship** between the measured emission radiance and the unknown H density (n_H) integrated along a viewing line-of-sight.

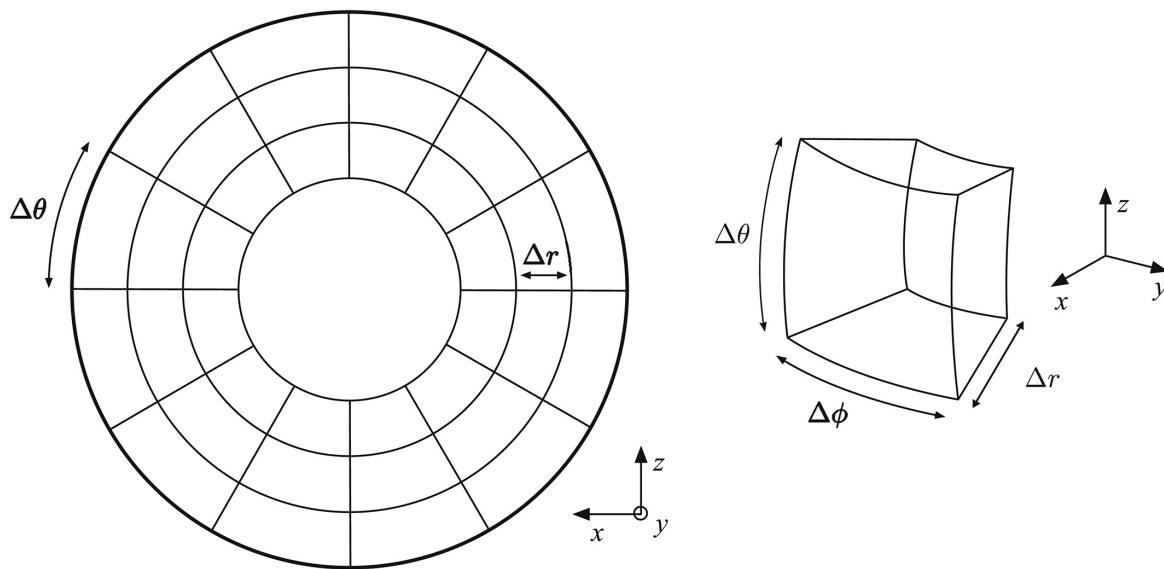


Radiative transfer equation for the optically thin region:

$$I(r, \hat{n}, t) = \frac{g^*}{10^6} \int_0^{L_{max}} n_H(l, t) \Psi(\beta) dl + I_{IP}(\hat{n}, t)$$

- $g^* \Rightarrow$ contains cross-section interaction and solar Ly- α flux.
- $n_H(l, t) \Rightarrow$ Hydrogen density in units of cm^{-3} .
- $\Psi(\beta) \Rightarrow$ Phase function due to the anisotropy scattering.
- $I_{IP} \Rightarrow$ Interplanetary background.
- $\hat{n}_i \Rightarrow$ LOS direction.
- $r \Rightarrow$ Tangential distance of a LOS.

The tomographic approach states that the volume of interest should be divided into voxels with a constant H density number. In this work, we adopt $\Delta r = 0.3125 R_E$, $\Delta \theta = 15 \text{ deg}$ and $\Delta \phi = 15 \text{ deg}$ yielding 6912 spherical voxels.



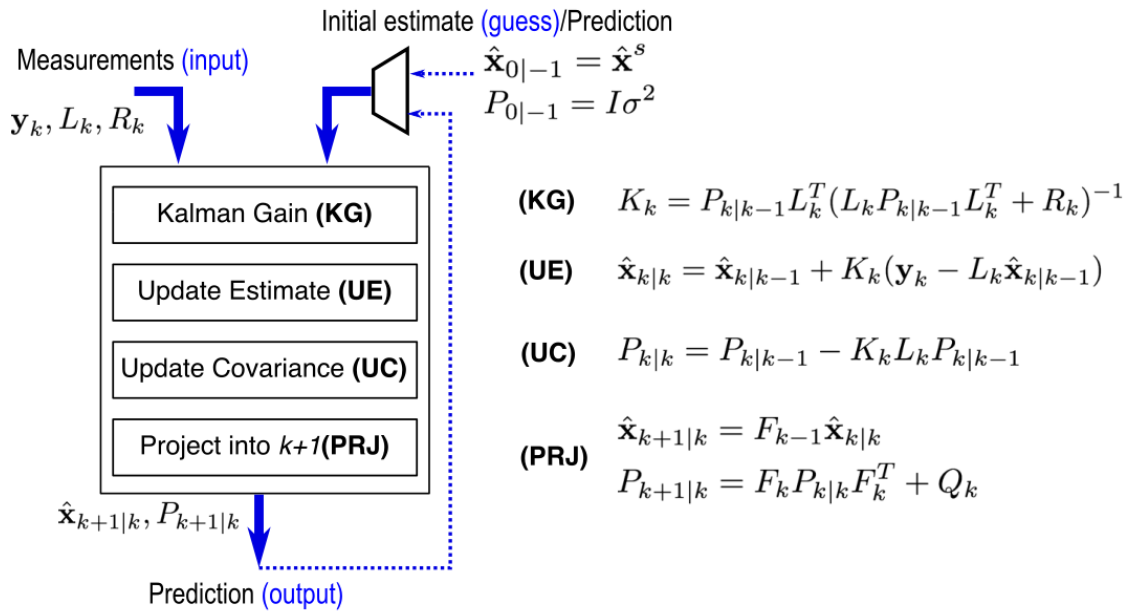
- After the spatial discretization into spherical voxels is performed, the radiative transfer equation adopts the form:

$$\mathbf{y} = L\mathbf{x}$$

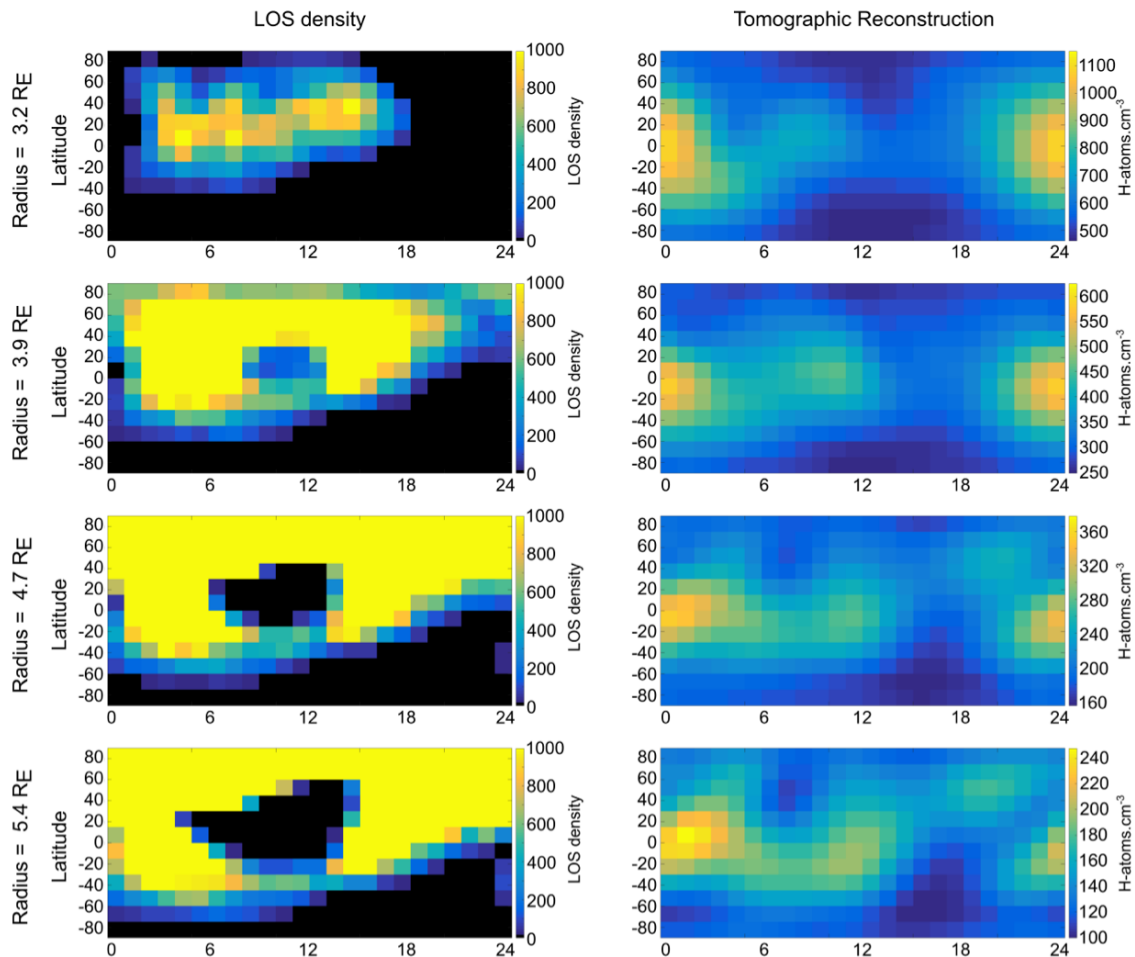
where:

- $\mathbf{y} \Rightarrow$ (**known**) the measurement vector generated by $I-I_{IP}$
 - $L \Rightarrow$ (**known**) the observation matrix generated with LOS direction, satellite position, voxel dimension, and solar Ly- α flux data.
 - $\mathbf{x} \Rightarrow$ (**unknown**) the vector that contains the H density number per voxel.
- Static tomographic reconstruction \mathbf{x}^s can be performed during quiet-time conditions using all available data and solving the expression above. During storm-time, a time-dependent model should be used $\mathbf{y}_k = L_k \mathbf{x}_k$ such that the input data stream may generate sequential reconstructions \mathbf{x}^d every time k .
 - Kalman Filter has been used to estimate the 3-D, **time-dependent** H density distribution from Ly- α emission. We used a **two-hour period** for reconstructions.

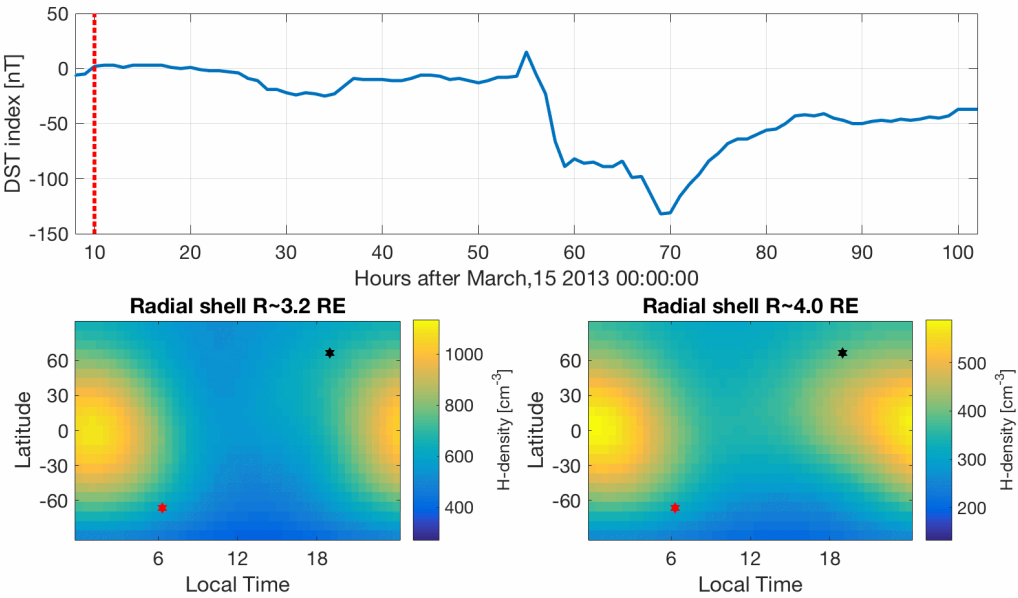
Kalman Filter Algorithm



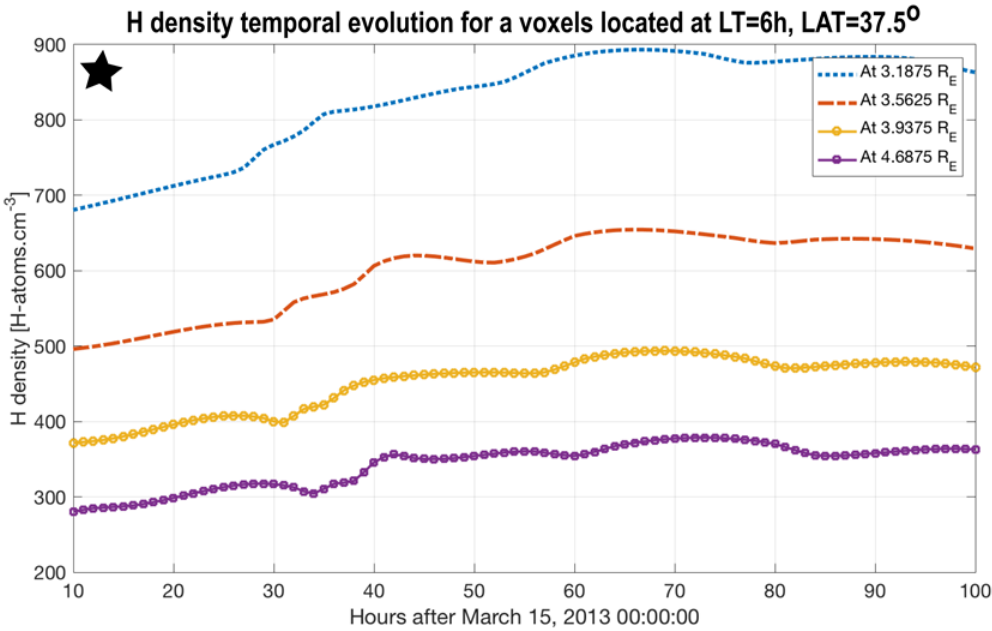
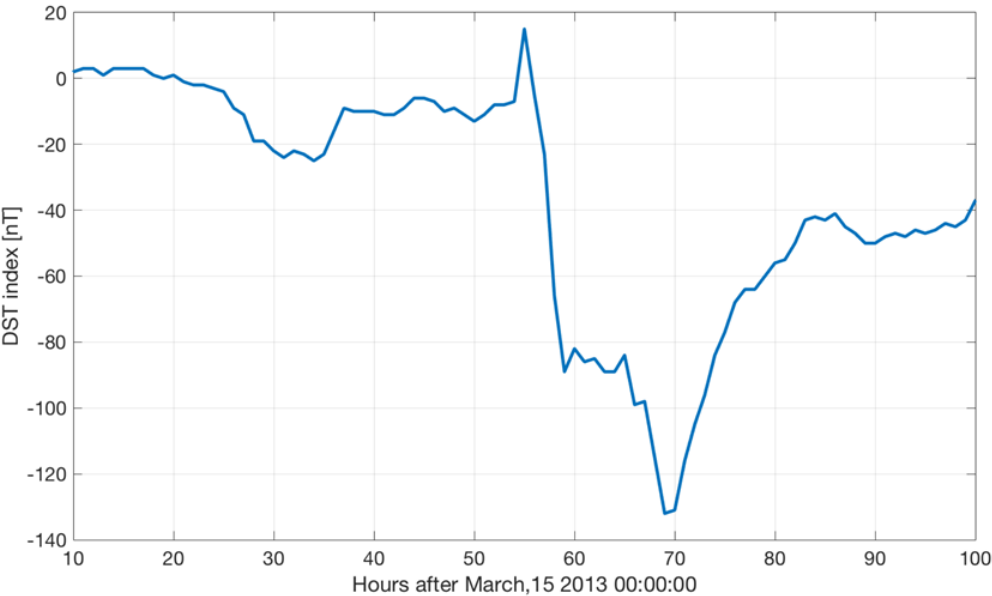
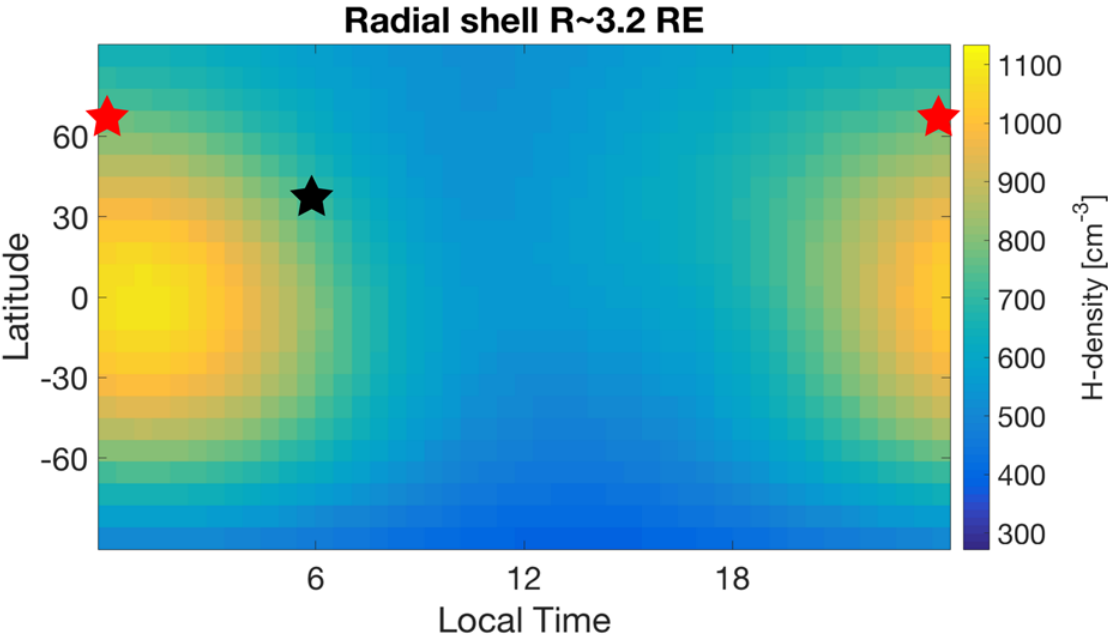
● The initial estimate $\hat{\mathbf{x}}^s$ is obtained by performing a static tomographic reconstruction using TWINS data for October-December 2012 during quiet-time conditions [Cucho-Padin & Waldrop, 2018 (<https://doi.org/10.1029/2018JA025323>)].

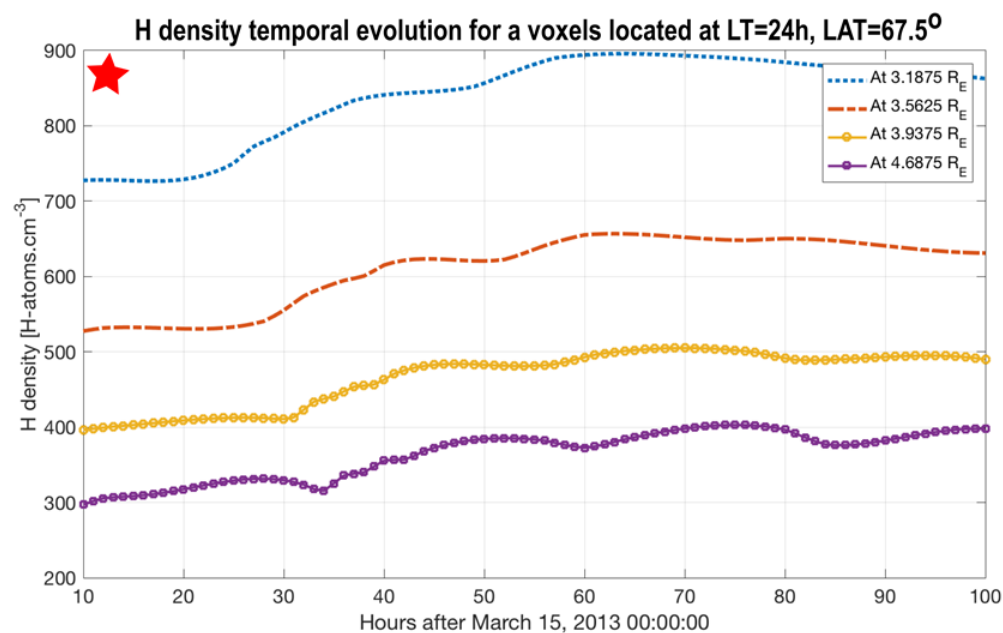


● Dynamic tomographic reconstruction during the storm occurred on March 17, 2013 [Cucho-Padin & Waldrop, 2019 (https://doi.org/10.1029/2019GL084327)].



● Temporal evolution of the H density for selected spatial locations.





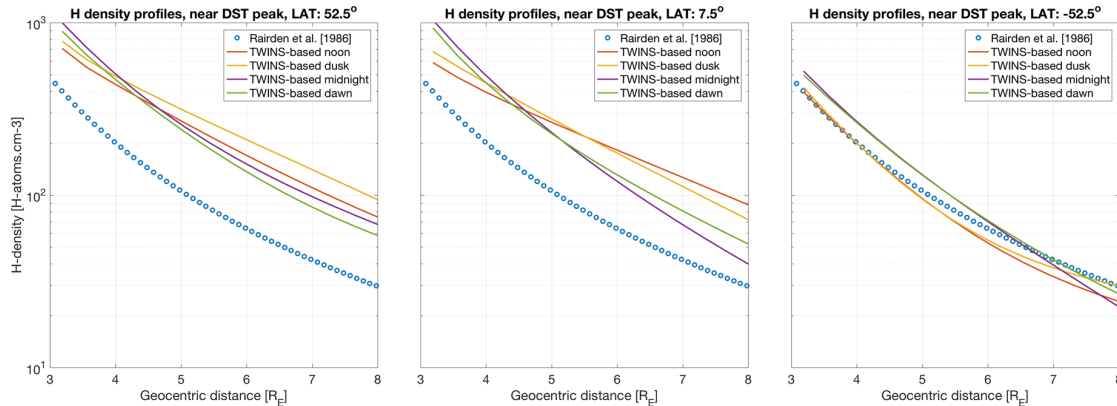
Highlights

- ✓ The temporal evolution of the H density shows a **~23%** increment (at the peak ~70h after March 15) with respect to quiet-time.
- ✓ Analysis of H density at different altitudes shows an **outward propagation** of H atoms.
- ✓ A constant increment of H density starting at ~30h after March 15 reveals that even **small geomagnetic variations** (DST~-30nT) can trigger an increased H escape.
- ✓ The balance of injection and loss of H atoms in this region is affected by **exosphere-plasmasphere interaction and thermospheric variations** [Kuwabara et al., 2017 (<https://doi.org/10.1002/2016JA023247>)]

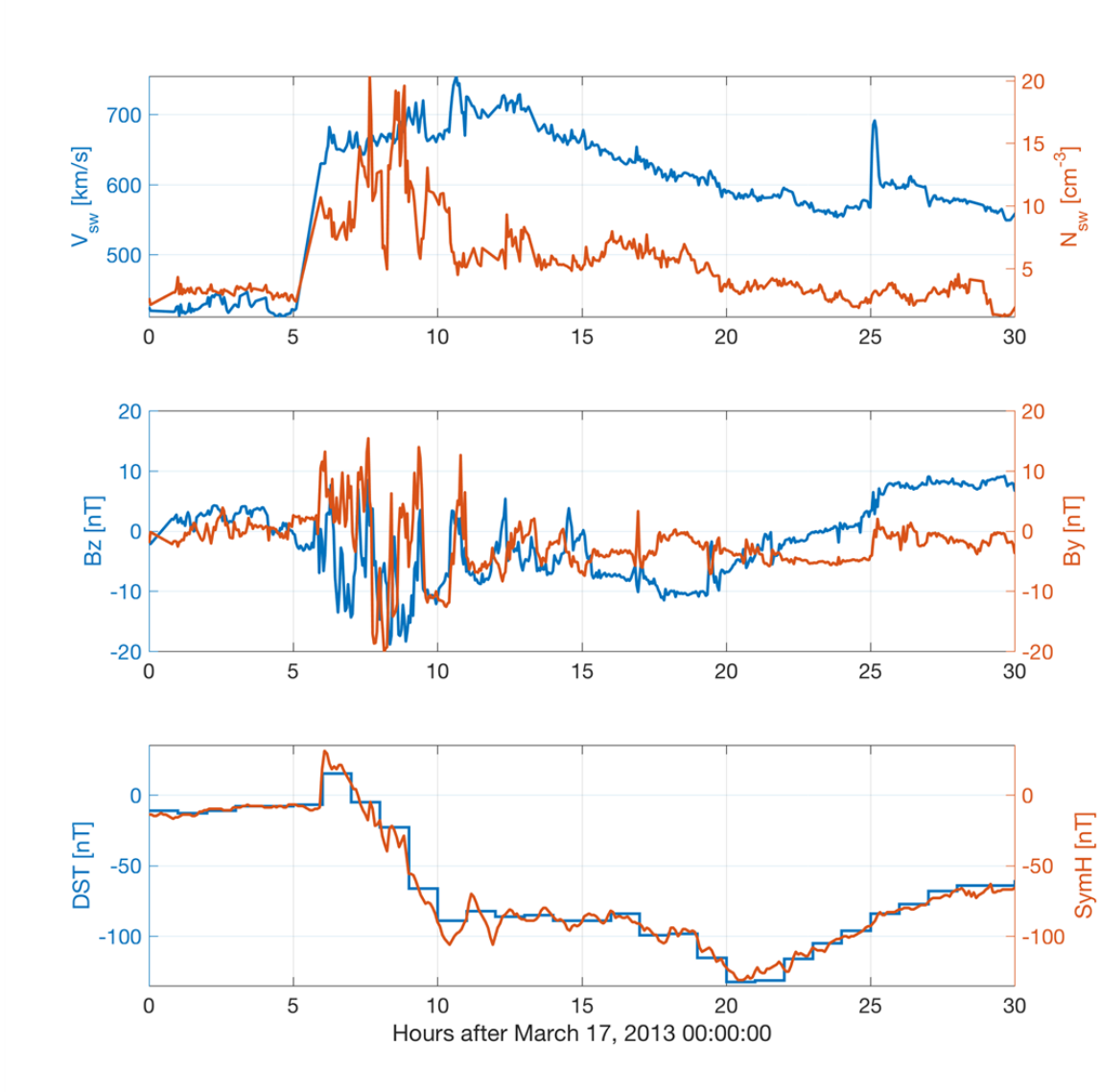
4. SIMULATIONS OF THE RING CURRENT DURING STORM-TIME

Incorporating the dynamic H profile into the CIMI model

- We analyze the ring current evolution using a **static H** density profile [Rairden et al., 1986 (<https://doi.org/10.1029/JA091iA12p13613>)] and our **dynamic H** density derived from Ly- α emission (TWINS/GUVI).

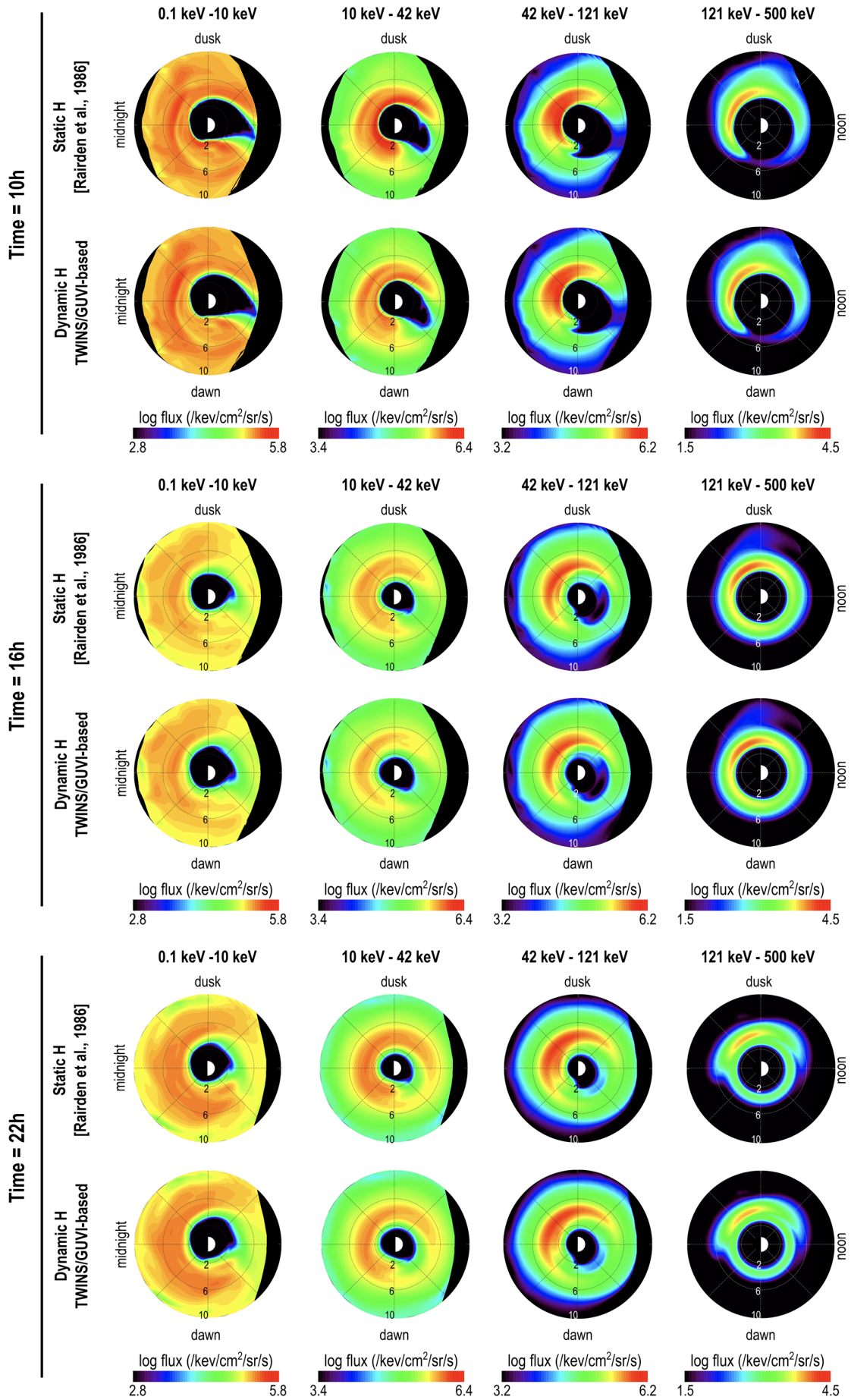


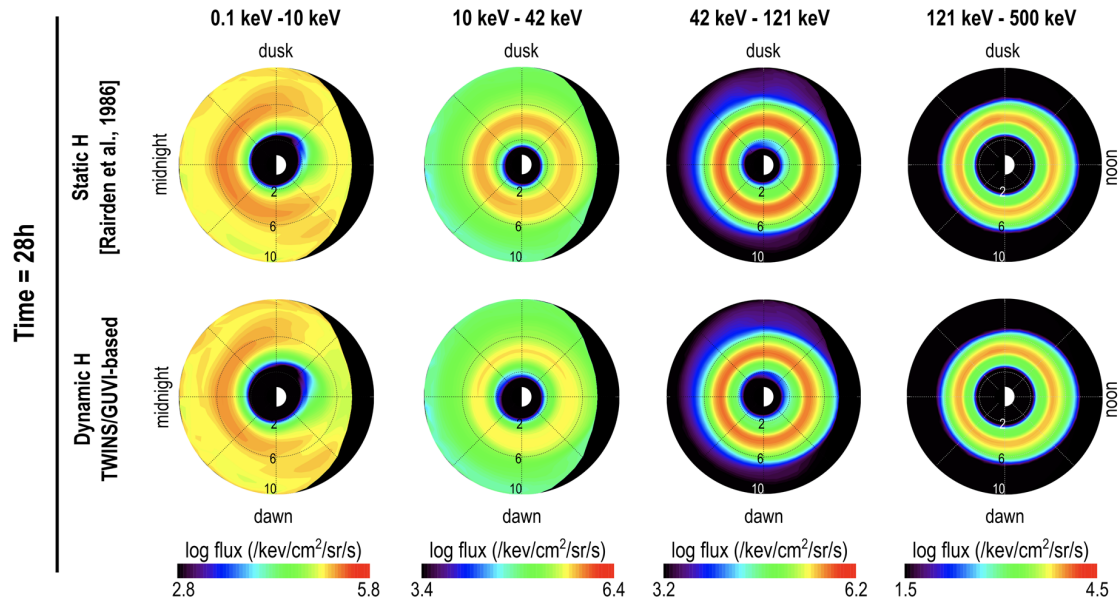
- We conduct CIMI simulations starting on **March 17, 2013**, for a period of ~ 30 hours.
 - Plasmasheet boundary of [Tsyganenko and Mukai, 2003 (<http://doi.org/10.1029/2002JA009707>)]
 - Ion species: H^+ , O^+
 - The Weimer 2K model [Weimer, 2001 (<http://doi.org/10.1029/2000JA000604>)] was used to determine the potential at CIMI's polar boundary.
 - The Model of [Hardy et al., 1987 (<http://doi.org/10.1029/JA092iA11p12275>)] was used to specify auroral conductance.
- Solar wind input data for CIMI simulations



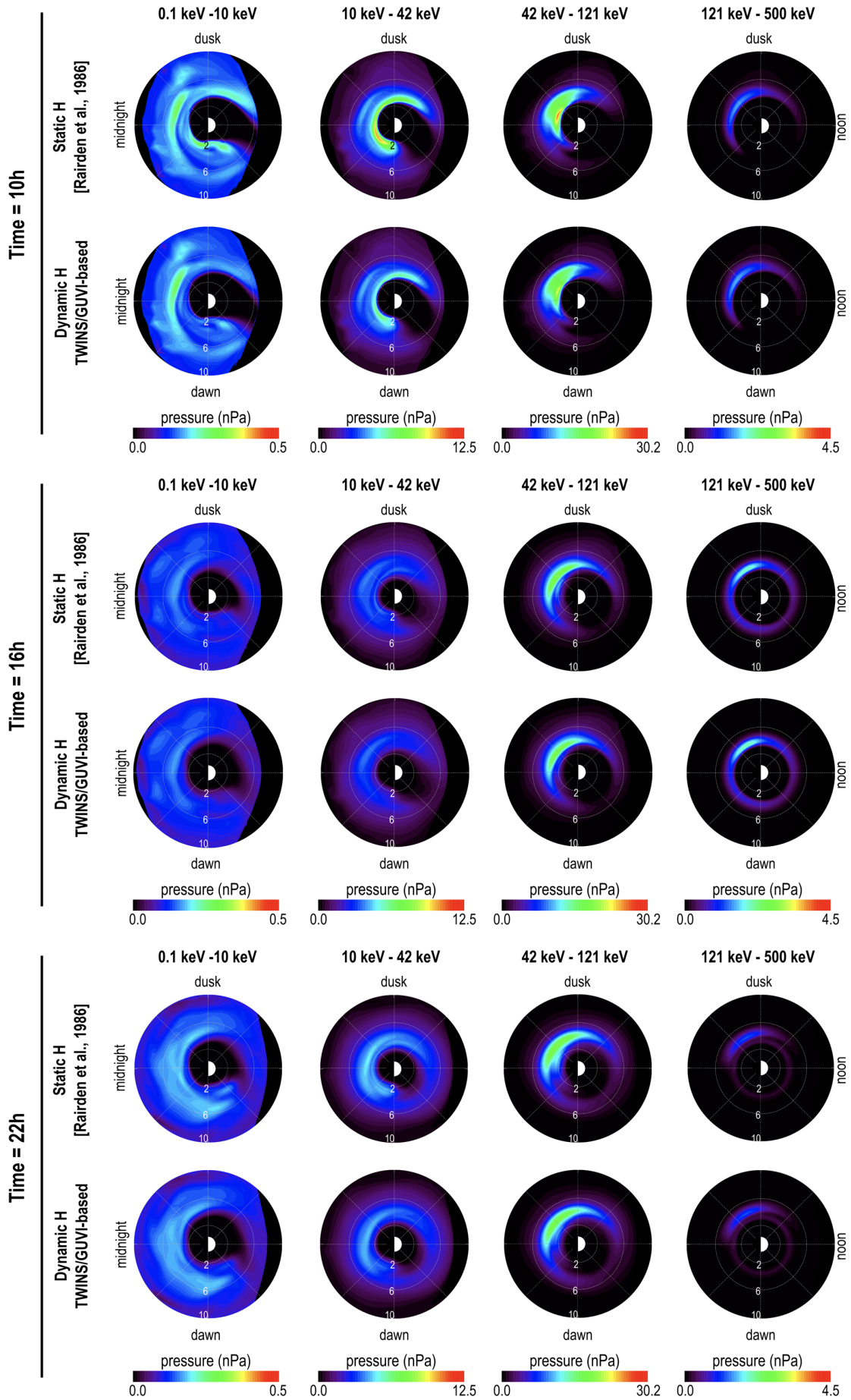
Temporal evolution of ring current ion flux and pressure

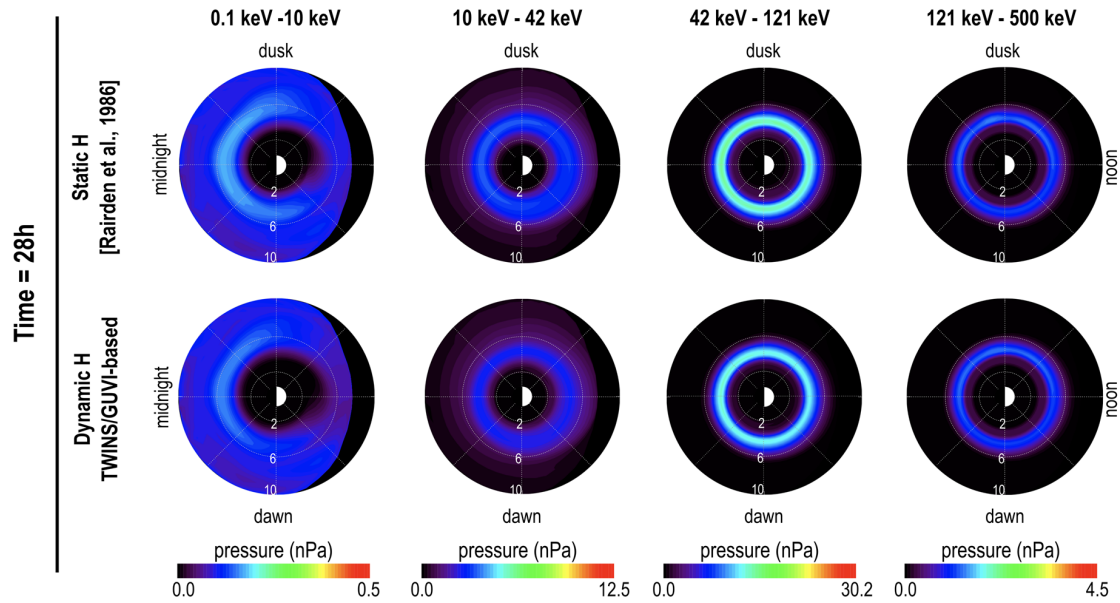
● Ring current H⁺ flux in the equatorial plane.



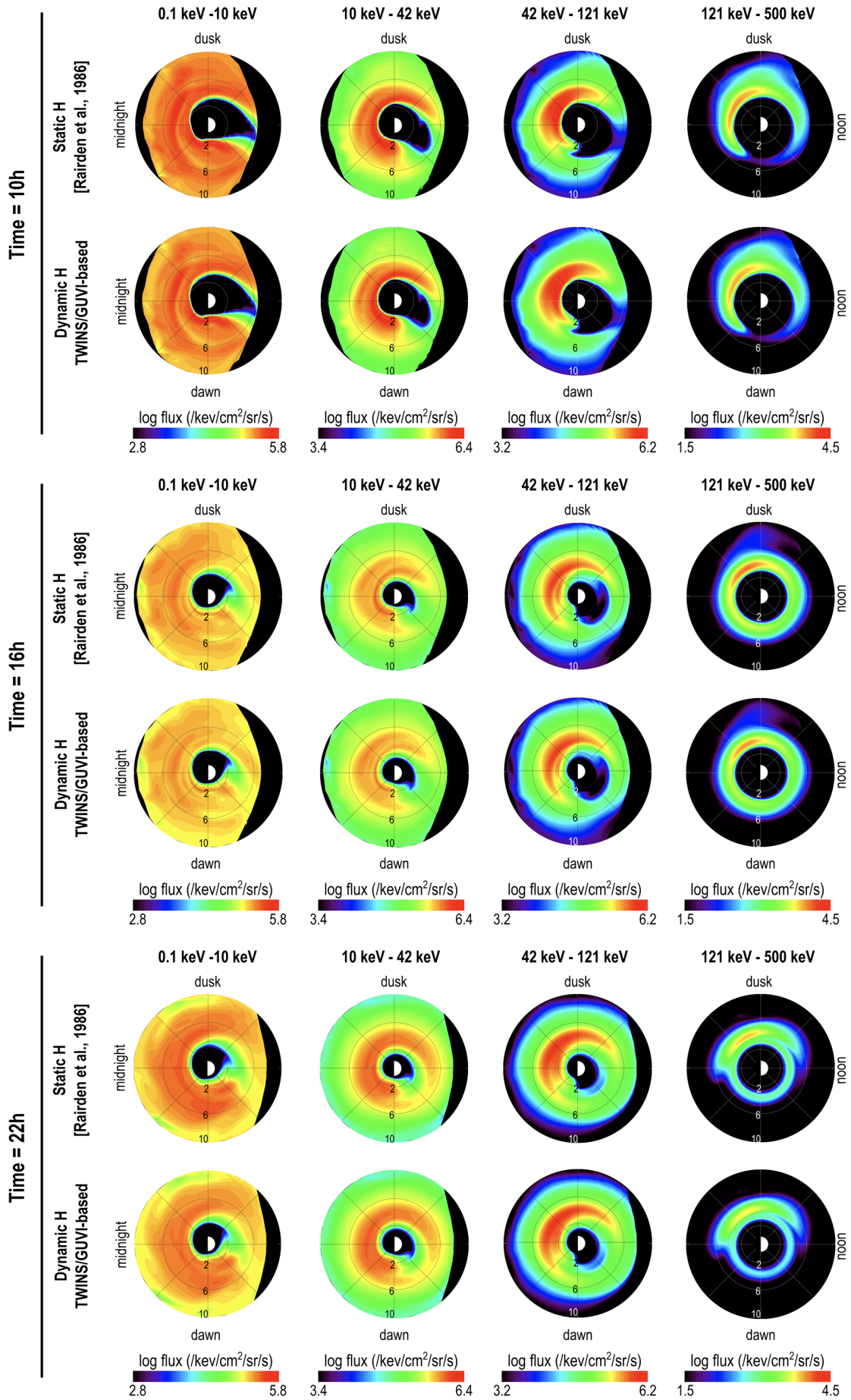


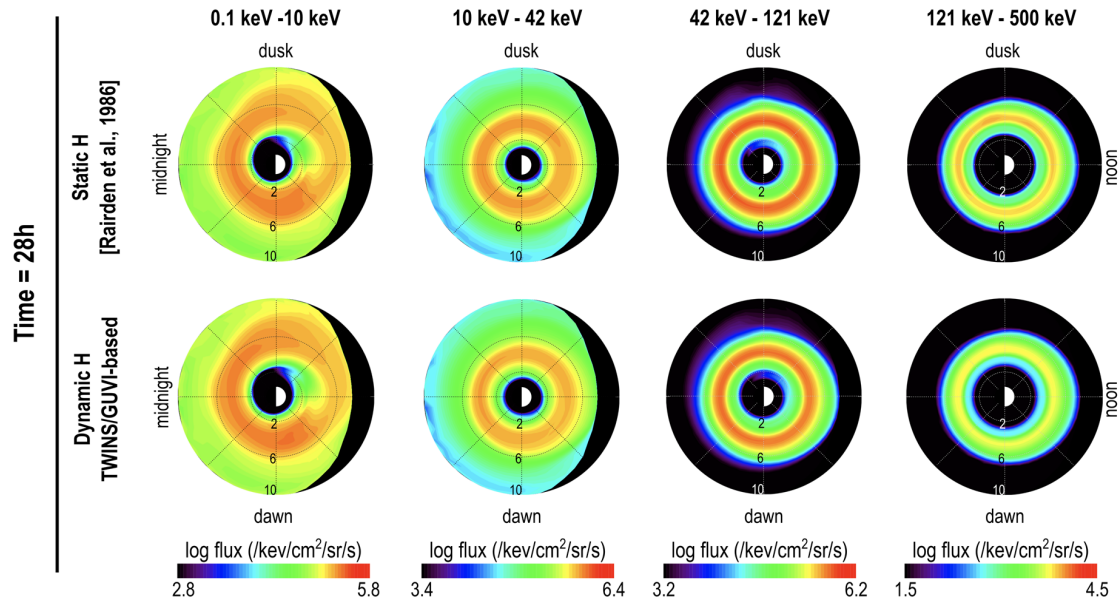
● Ring current H⁺ pressure in the equatorial plane.



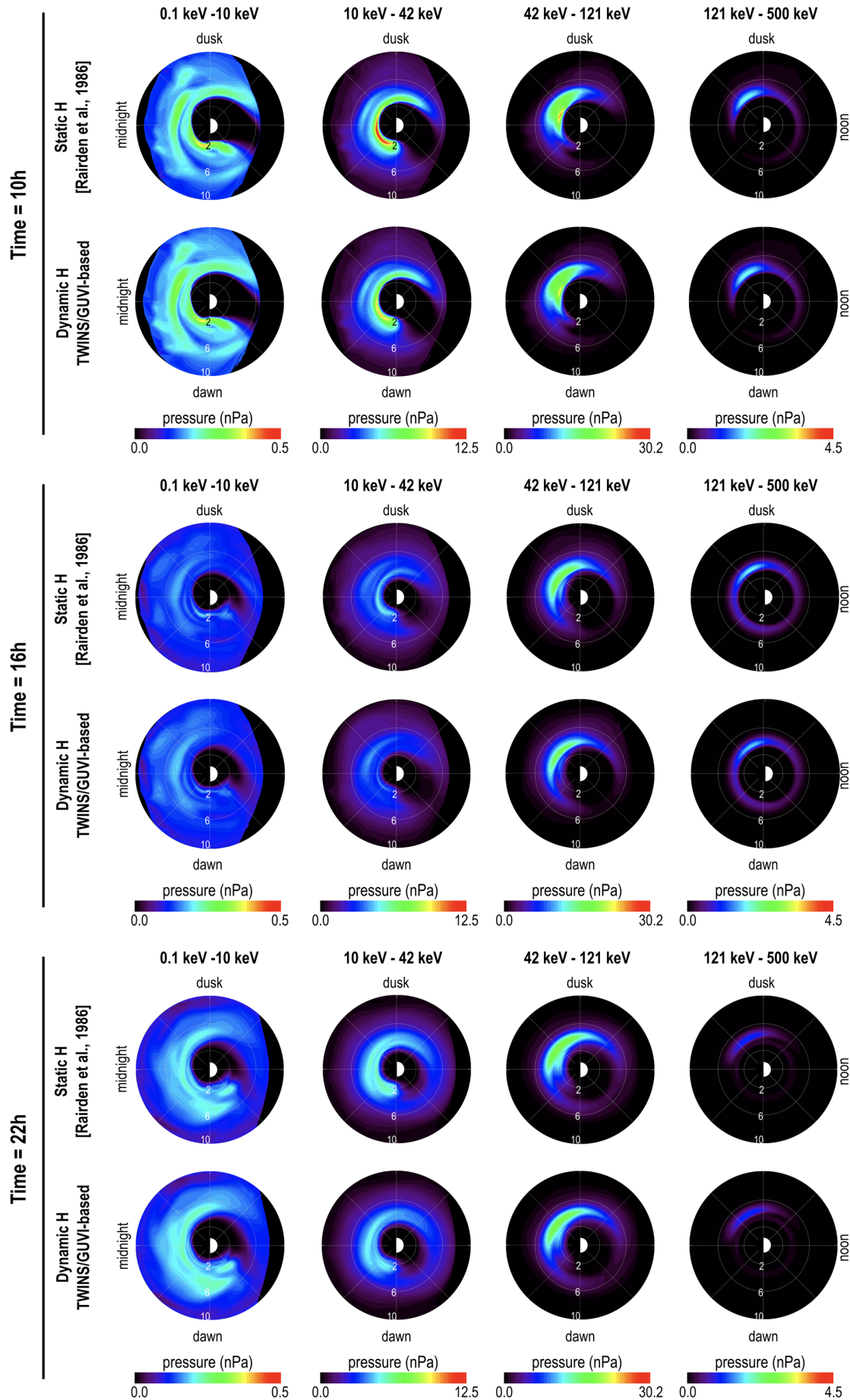


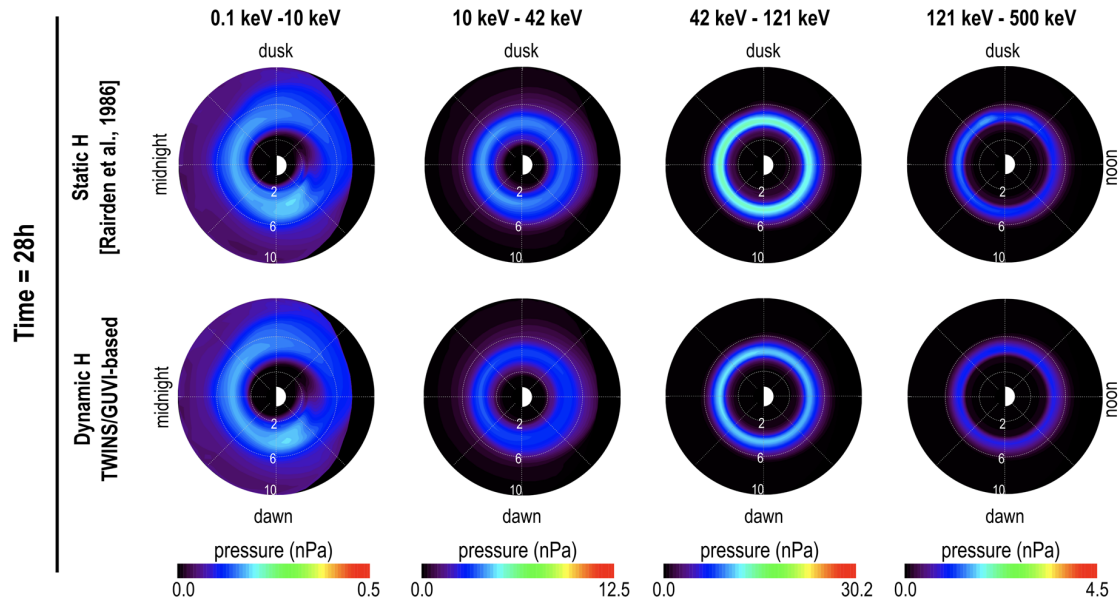
● Ring current O⁺ flux in the equatorial plane.





● Ring current O⁺ pressure in the equatorial plane.





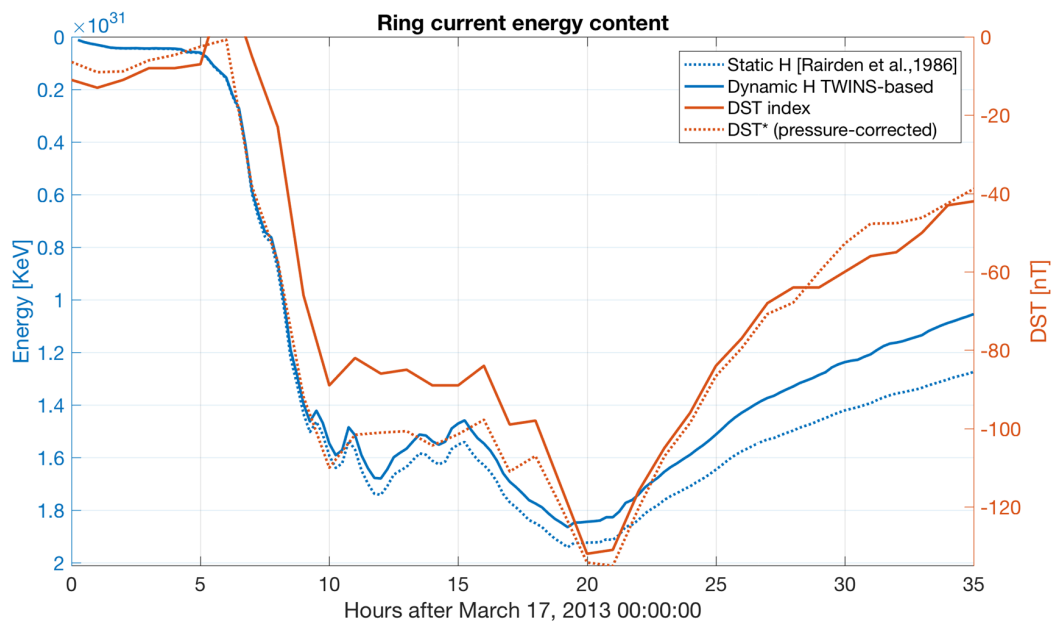
Highlights

- ✓ Ring current H^+ flux present evident **structural variations in the energy range 10 keV - 42 keV** during the development of the storm. The corresponding cross-section for this energy range seems to be more effective to produce charge-exchange events. (NOTE: log10 scale used for flux)
- ✓ Depletion of H^+ flux occurs mainly in the nightside-dawn region, where atomic H density tends to be higher.

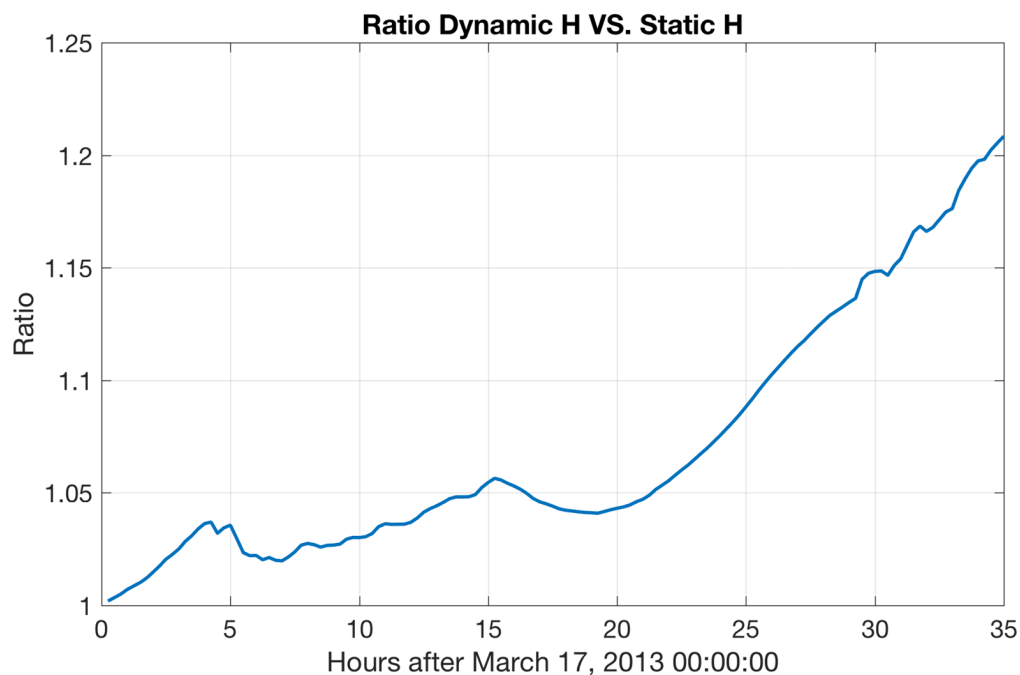
5. RING CURRENT RECOVERY RATE ANALYSIS

Temporal variation of the total ring current energy content

- Estimation of recovery rates for each exospheric H density model.



- By analyzing the ratio between the two energy content curves, we can quantitatively measure how fast is the recovery rate when the dynamic H profile is used with respect to the use of the static H profile.



- In the last 5 hours, the recovery rate for the static H and dynamic H cases was **0.816 keV.d⁻¹** and **0.960 keV.d⁻¹**, respectively.

Highlights

✓ The use of the **dynamic H** density distributions presents a higher recovery rate than the use of the static H density. The ratio plot shows the tendency to a higher rate as the storm evolves.

6. CONCLUSIONS

Conclusions

- ✓ In this work, we have developed a tomographic technique to estimate time-dependent H density distributions during storm-time from Ly- α emission, and it has been used to assess the ring current recovery rate.
- ✓ The temporal variation of the ring current total energy content for a given species has been used to estimate the recovery rate.
- ✓ We found a quantitative that the dynamic H density yields a faster recovery rate. These results are in good agreement with those reported by [Kroll et al, 2018 (<http://agupubs.onlinelibrary.wiley.com/doi/full/10.1002/2017SW001780>)] and [Ilie et al, 2012 (<http://doi.org/10.1016/j.jastp.2012.03.010>)] where higher H density results in an increased charge-exchange loss of ring current ions.
- ✓ These results emphasize the importance of an accurate estimation of exospheric H density and the need for satellite-based missions to specifically measure the exosphere. The Global Lyman-alpha Imagers for the Dynamic Exosphere (GLIDE) mission led by Dr. Waldrop, has been accepted for launch in 2024. It will provide wide-field global images of the exosphere with a 30-min temporal resolution.

Acknowledgment

The authors thank Dr. Dolon Battacharya for helping in running the simulations.

ABSTRACT

Atomic Hydrogen (H) is the most abundant constituent of the terrestrial exosphere. Its charge exchange interaction with ring current ions (H^+ and O^+) serves to dissipate magnetospheric energy during geomagnetic storms, resulting in the generation of energetic neutral atoms (ENAs). Determination of ring current ion distributions through modeling depends critically on the specification of the exospheric H density distribution. Furthermore, theoretical studies have demonstrated that ring current recovery rate after the storm onset directly correlates with the H density. Although measurements of H airglow emission at altitudes [3,6] Re exhibit storm-time variations, the H density distributions used in ring current modeling are typically assumed to be temporally static during storms. In this presentation, we will describe the temporal and spatial evolution of ring current ion densities in response to a realistically dynamic exospheric H density distribution using the Comprehensive Inner Magnetosphere-Ionosphere Model (CIMI). The exospheric densities used as input to the model are fully data-driven, derived as global, 3D, and time-dependent tomographic reconstructions of H emission data acquired from Lyman-alpha detectors onboard the NASA TWINS satellites during the geomagnetic storm that occurred on March 17, 2013. We will examine modeled ring current recovery rates using both dynamic and static reconstructions and evaluate the impact of realistic storm-time exospheric variability on the simulations.

REFERENCES

- Fok, M.-C., Buzulukova, N. Y., Chen, S.-H., Glocer, A., Nagai, T., Valek, P., and Perez, J. D. (2014), The Comprehensive Inner Magnetosphere-Ionosphere Model, *J. Geophys. Res. Space Physics*, 119, 7522– 7540, doi:10.1002/2014JA020239.
- Krall, J., Glocer, A., Fok, M.-C., Nossal, S. M., & Huba, J. D. (2018). The unknown hydrogen exosphere: Space weather implications. *Space Weather*, 16, 205– 215. <https://doi.org/10.1002/2017SW001780>
- R. Ilie, R.M. Skoug, H.O. Funsten, M.W. Liemohn, J.J. Bailey, M. Gruntman (2013) The impact of geocoronal density on ring current development, *Journal of Atmospheric and Solar-Terrestrial Physics*, vol 99, pp 92-103,
- Bailey, J., and Gruntman, M. (2011), Experimental study of exospheric hydrogen atom distributions by Lyman- α detectors on the TWINS mission, *J. Geophys. Res.*, 116, A09302, doi:10.1029/2011JA016531.
- Zoennchen, J. H., et al. (2015) "Terrestrial exospheric hydrogen density distributions under solar minimum and solar maximum conditions observed by the TWINS stereo mission." *Annales Geophysicae*, vol. 33, no. 3, p. 413.
- Hodges, R. R. (1994), Monte Carlo simulation of the terrestrial hydrogen exosphere, *J. Geophys. Res.*, 99(A12), 23229-23247, doi:10.1029/94JA02183.
- Zoennchen, J. H., Nass, U., Fahr, H. J., and Goldstein, J.: The response of the H geocorona between 3 and 8 Re to geomagnetic disturbances studied using TWINS stereo Lyman- α data, *Ann. Geophys.*, 35, 171–179, <https://doi.org/10.5194/angeo-35-171-2017>, 2017.
- Kuwabara, M., Yoshioka, K., Murakami, G., Tsuchiya, F., Kimura, T., Yamazaki, A., and Yoshikawa, I. (2017), The geocoronal responses to the geomagnetic disturbances, *J. Geophys. Res. Space Physics*, 122, 1269– 1276, doi:10.1002/2016JA023247.
- McComas, D.J., Allegrini, F., Baldonado, J. et al. (2009) The Two Wide-angle Imaging Neutral-atom Spectrometers (TWINS) NASA Mission-of-Opportunity. *Space Sci Rev* 142, 157–231. <https://doi.org/10.1007/s11214-008-9467-4>
- Qin, J., Waldrop, L., and Makela, J. J. (2017), Redistribution of H atoms in the upper atmosphere during geomagnetic storms, *J. Geophys. Res. Space Physics*, 122, 10,686– 10,693, doi:10.1002/2017JA024489.
- Østgaard, N., Mende, S. B., Frey, H. U., Gladstone, G. R., and Lauche, H. (2003), Neutral hydrogen density profiles derived from geocoronal imaging, *J. Geophys. Res.*, 108, 1300, doi:10.1029/2002JA009749, A7.
- Cucho-Padin, G., & Waldrop, L. (2018). Tomographic estimation of exospheric hydrogen density distributions. *Journal of Geophysical Research: Space Physics*, 123, 5119– 5139. <https://doi.org/10.1029/2018JA025323>
- Cucho-Padin, G., & Waldrop, L. (2019). Time-dependent response of the terrestrial exosphere to a geomagnetic storm. *Geophysical Research Letters*, 46, 11661– 11670. <https://doi.org/10.1029/2019GL084327>
- Rairden, R. L., Frank, L. A., and Craven, J. D. (1986), Geocoronal imaging with Dynamics Explorer, *J. Geophys. Res.*, 91(A12), 13613– 13630, doi:10.1029/JA091iA12p13613.
- Tsyganenko, N. A., and Mukai, T. (2003), Tail plasma sheet models derived from Geotail particle data, *J. Geophys. Res.*, 108, 1136, doi:10.1029/2002JA009707, A3.
- Weimer, D. R. (2001), An improved model of ionospheric electric potentials including substorm perturbations and application to the Geospace Environment Modeling November 24, 1996, event, *J. Geophys. Res.*, 106(A1), 407– 416, doi:10.1029/2000JA000604.
- Hardy, D. A., Gussenhoven, M. S., Raistrick, R., and McNeil, W. J. (1987), Statistical and functional representations of the pattern of auroral energy flux, number flux, and conductivity, *J. Geophys. Res.*, 92(A11), 12275– 12294, doi:10.1029/JA092iA11p12275.